



# Aerosol indirect effects on the temperature-precipitation scaling

Nicolas Da Silva<sup>1</sup>, Sylvain Mailler<sup>1,2</sup>, and Philippe Drobinski<sup>1</sup>

<sup>1</sup>LMD/IPSL, École polytechnique, Université Paris Saclay, ENS, PSL Research University, Sorbonne Universités, UPMC Univ Paris 06, CNRS, Palaiseau, France

<sup>2</sup>ENPC, Champs-sur-Marne, France

**Correspondence:** Nicolas Da Silva ([nicolas.da-silva@lmd.polytechnique.fr](mailto:nicolas.da-silva@lmd.polytechnique.fr))

## Abstract.

Indirect effects of aerosols were found to weaken convective precipitation through reduced precipitable water and convective instability. The present study aims at quantifying the relative importance of these two processes in the reduction of summer precipitation using the temperature-precipitation scaling. Based on a numerical sensitivity experiment conducted over central Europe aiming to isolate indirect effects, all others effects being equal, the results show that the scaling of hourly convective precipitation with temperature follows the Clausius-Clapeyron (CC) relationship whereas the decrease of convective precipitation does not scale with the CC law since it is mostly attributable to increased stability with increased aerosols concentrations rather than to decreased precipitable water content. This effect is larger at low temperatures for which clouds are statistically more frequent and optically thicker. At these temperatures, the increase of stability is mostly linked to the stronger reduction of temperature in the lower troposphere compared to the upper troposphere which results in lower lapse rates.

## 1 Introduction

The temperature-precipitation relationship has often been studied because it has been hypothesised to give an insight of the change of precipitation in a warming climate. In this context, one may distinguish extreme precipitation studies from mean precipitation studies. The Clausius-Clapeyron (CC) relation is a first guess for the temperature-precipitation extremes scaling because it relates changes in temperature to changes in water vapor content assuming constant relative humidity:

$$\frac{\partial e_s}{\partial T} = \frac{L_v e_s}{R_v T^2} \quad (1)$$

where  $e_s$  is the water vapor saturation pressure,  $T$  is the temperature,  $L_v$  is the latent heat of vaporization and  $R_v$  is the gas constant for air. However many departures from the CC-scaling have been observed. Literature has described a hook shape for the temperature-precipitation extremes relationship with CC-scaling for the cold season and negative scaling for the warm season (Drobinski et al., 2016). Sub-CC scaling for warm temperatures can be explained by either the decrease of relative humidity (Hardwick et al., 2010; Panthou et al., 2014), the decrease of precipitation duration (Utsumi et al., 2011; Singleton and Toumi, 2013; Panthou et al., 2014), the decrease of precipitation efficiency or changes in dynamics (Drobinski et al., 2016). Conversely, Lenderink and van Meijgaard (2008) has found an increase of precipitation extremes beyond the CC-scaling for temperatures between 12°C and 23°C at de Bilt in Netherlands. It has been argued that this "super-CC" scaling is due to the



transition between stratiform and convective precipitation (Haerter and Berg, 2009; Berg and Haerter, 2013; Molnar et al., 2015) and enhanced dynamics in convective clouds at higher temperatures (Lenderink et al., 2017). Although less documented than extremes, a hook shape is also suggested for mean precipitation (Zhao and Khalil, 1993; Madden and Williams, 1978; Lenka and Eva, 2017; Rodrigo, 2018) as well as differences between land and sea areas (Adler et al., 2008; Trenberth and 5 Shea, 2005). Hardwick et al. (2010) have systematically found lower slopes for median precipitation with respect to extreme precipitation in their 4 studied areas in Australia.

The fact that the CC law is not always adequate for describing the temperature-precipitation relationship in a given climate does not mean that if one would perturb the climate, the change in precipitation would not follow a CC-scaling. Indeed, using Regional Climate Models (RCM) in the Mediterranean region and within the frame of the HyMeX program (Drobinski et al., 10 2014), Drobinski et al. (2018) found a CC-scaling between past and future climate while observing hook shapes for both past and future climate temperature-precipitation relationships. It has often been shown that extreme precipitation would increase at a rate similar to the CC law whereas mean precipitation would increase at a lower rate in a warming climate (Allen and Ingram, 2002; Boer, 1993; Trenberth, 1998; Held and Soden, 2006).

Apart from the greenhouse gases forcing, the forcing of aerosols is another feature that can modify climate and therefore 15 temperature-precipitation relationship. Aerosols affect climate through their direct and semi-direct effects as well as through their effects on cloud microphysics (indirect effects). While their direct effect is rather well understood, many uncertainties remain for the indirect effects. Stevens and Feingold (2009) described aerosol cloud interactions as a buffered system in which many processes seem to partly compensate each other. Among these effects, the Twomey (1977) effect, also called "first indirect effect", is an increase of the Cloud Optical Depth (COD) through reduced cloud droplet radius with increased aerosol 20 concentrations. Aerosols indirect effects may also increase cloud lifetime (Albrecht, 1989) but as of today no consensus exists on the reality of this effect (Small et al., 2009; Seifert et al., 2015), and its representation in climate models is highly dependent on the model's microphysical formulation (Zhou and Penner, 2017). An invigoration effect has been diagnosed for convective precipitation (Fan et al., 2013) through an increased release of latent heat due to ice formation associated with a decrease of warm rain formation with increased aerosol loads.

25 A common feature of both direct and indirect effects of aerosols is a global decrease of precipitation through a decrease of evaporation due to the reduction of shortwave downwelling fluxes at the surface (Ramanathan et al., 2001; Lelieveld et al., 2002; Bollasina et al., 2011; Salzmann et al., 2014). In their study of aerosol indirect effects over the Euro-Mediterranean area, Da Silva et al. (2018) diagnosed the same path for their simulated decrease of precipitation (see Figure 1). They have shown that the consecutive surface cooling not only reduces the water content but also stabilizes the atmosphere as suggested by Fan et al. 30 (2013); Morrison and Grabowski (2011), and hence acts in reducing precipitation with increased aerosol concentrations. A third path is possible as a combination of these two paths since the reduction of water vapor mixing ratio at the surface would also contribute to increase the stability of the atmosphere through less latent heat released with increased aerosol concentrations. To our knowledge, an evaluation of the relative contribution of these paths to precipitation reduction due to aerosol indirect effects has not been proposed yet. This study aims at determining these contributions and therefore can be seen as a natural

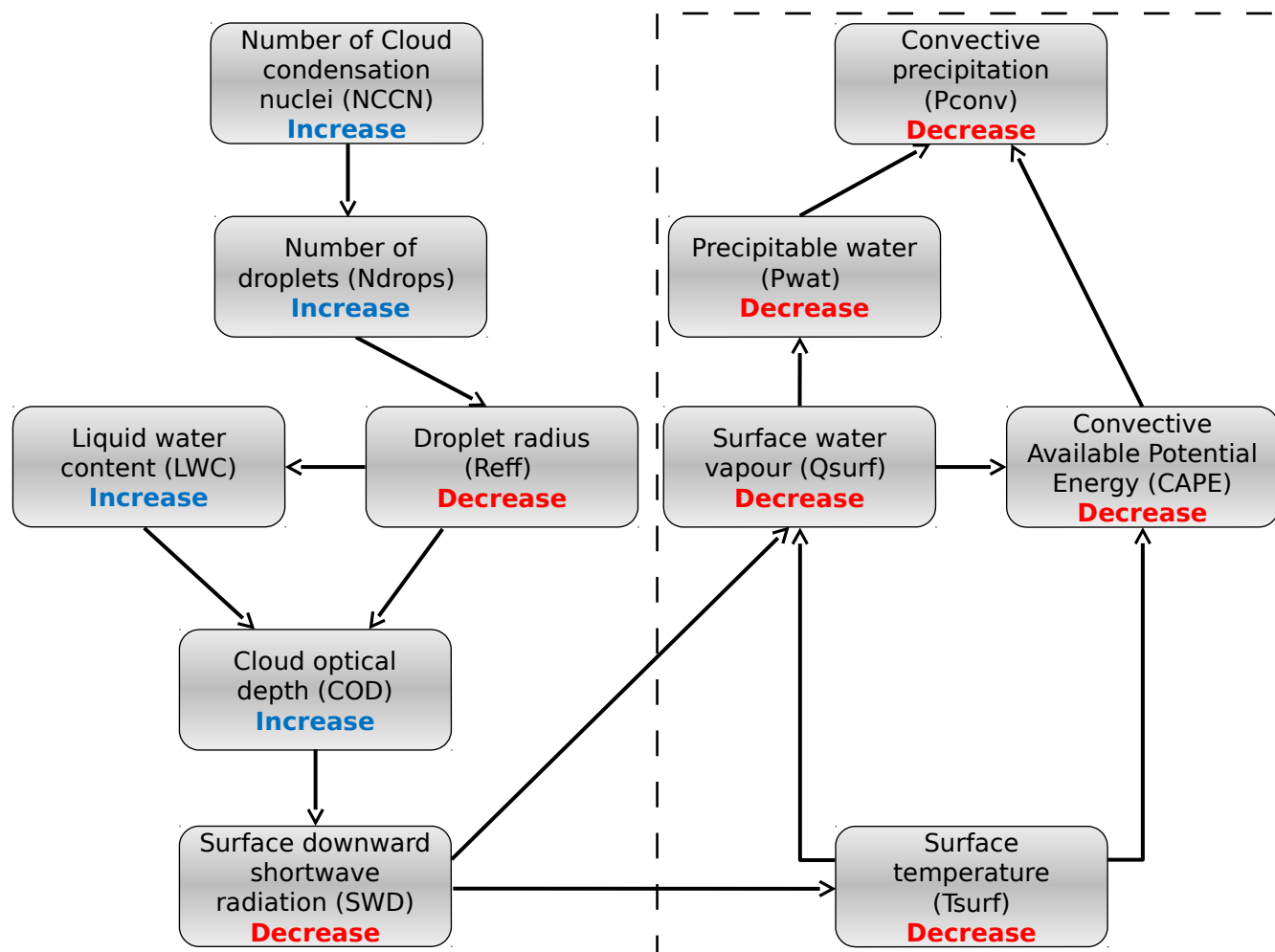


**Figure 1.** Schematic summary of the aerosol causal sequence for the indirect effects of aerosols on convective precipitation (from Da Silva et al. (2018)). The dotted rectangle indicates the part of the scheme which is detailed in the present study.

follow-up of Da Silva et al. (2018). For that purpose, we use the temperature-precipitation relationship which appears to be a natural framework since both effects are a consequence of the decrease of surface temperature.

Section 2 details the configuration of the WRF model used, the simulations, and the method that have been performed for this sensitivity analysis. Section 3 analyses the temperature-precipitation scaling and quantifies each contribution to the reduction of central Europe summertime precipitation under the effect of a massive concentration of cloud condensation nuclei. Section 4 concludes the study.



## 2 Methods

### 2.1 Model configuration

The version 3.7.1 of the Weather Research and Forecasting Model (WRF, Skamarock et al., 2008) is used in this study. The model was run with a 50 km (LR) and a 3.3 km (HR) horizontal resolution on a domain displayed in Fig. 2. It is forced by the Global Forecast System (GFS) model (National Centers for Environmental Prediction National Weather Service, 2000) as initial and boundary conditions. Temperature, humidity, geopotential and velocity components are nudged towards GFS analysis data with a Newtonian-type method using a relaxation coefficient of  $5 \times 10^{-5} \text{ s}^{-1}$  as recommended by, e.g., Salameh et al. (2010); Omrani et al. (2013, 2015).

The microphysical scheme used is the Thompson and Eidhammer (2014) scheme which explicitly calculates the number concentrations of aerosols. The latter are represented in a simplified way according to their capacity to nucleate cloud water ("water friendly", WFA) or ice water ("ice friendly", IFA). Aerosol number concentrations are initialized and forced at domain boundaries by a climatology based on Goddard Chemistry Aerosol Radiation and Transport (GOCART) model (Ginoux et al., 2001) simulations. While no surface emissions are applied to IFA, surface emission fluxes are applied to WFA in order to approximately equilibrate the loss of WFA due to scavenging and nucleation. The radiation scheme is RRTMG (Rapid Radiative Transfer Model for General circulation models, Iacono et al., 2008) and uses the cloud water droplets, ice and snow effective radii of the Thompson and Eidhammer (2014) microphysical scheme to resolve the radiative transfer equations. Another climatology of aerosols from Tegen et al. (1997) is used in this radiative scheme and therefore is not affected by any changes in the microphysical aerosol climatology, which enables us to perform sensitivity experiments of the indirect effects of aerosols with fixed aerosol direct effect. The Kain (2004) scheme is used to parameterize convection. The microphysical effects of aerosols are not taken into account explicitly in this parameterization although they can affect convection indirectly through modifications in the temperature or moisture profiles.

This configuration is the same as in Da Silva et al. (2018) to which the reader is referred for additional detail.

### 2.2 Simulation experiments

The model was run to make two extreme simulations in terms of WFA and IFA microphysical concentrations. Both simulations start on April 1<sup>st</sup>, 2013 (after one month of spin-up) and end on September 17, 2013. A very high aerosol emission level ( $1.75 \times 10^7 \text{ kg s}^{-1}$  for the whole domain) is applied in the first simulation, referred as MAX or polluted simulation and a very low aerosol emission level ( $1.75 \times 10^{-4} \text{ kg s}^{-1}$  for the whole domain) is applied for the other simulation, referred as MIN or pristine simulation. Although these emission rates are extreme, maximal and minimal value permitted by the microphysics scheme reduce the range of variation of the number of WFA (NWFA) between  $\sim 10 \text{ cm}^{-3}$  and  $\sim 10,000 \text{ cm}^{-3}$  and of the number of IFA (NIFA) between  $0.005 \text{ cm}^{-3}$  and  $10,000 \text{ cm}^{-3}$ . Therefore these latter extreme emission rates ensure that both NIFA and NWFA in the MIN (resp. MAX) simulation remain close to their minimal (resp. maximal) permitted values, which corresponds to a  $2 \times 10^6$  factor for NIFA and a  $10^3$  factor for NWFA between the MAX and the MIN simulations. Such high



### Apr.-Sep. conv. precipitation difference (MAX-MIN)

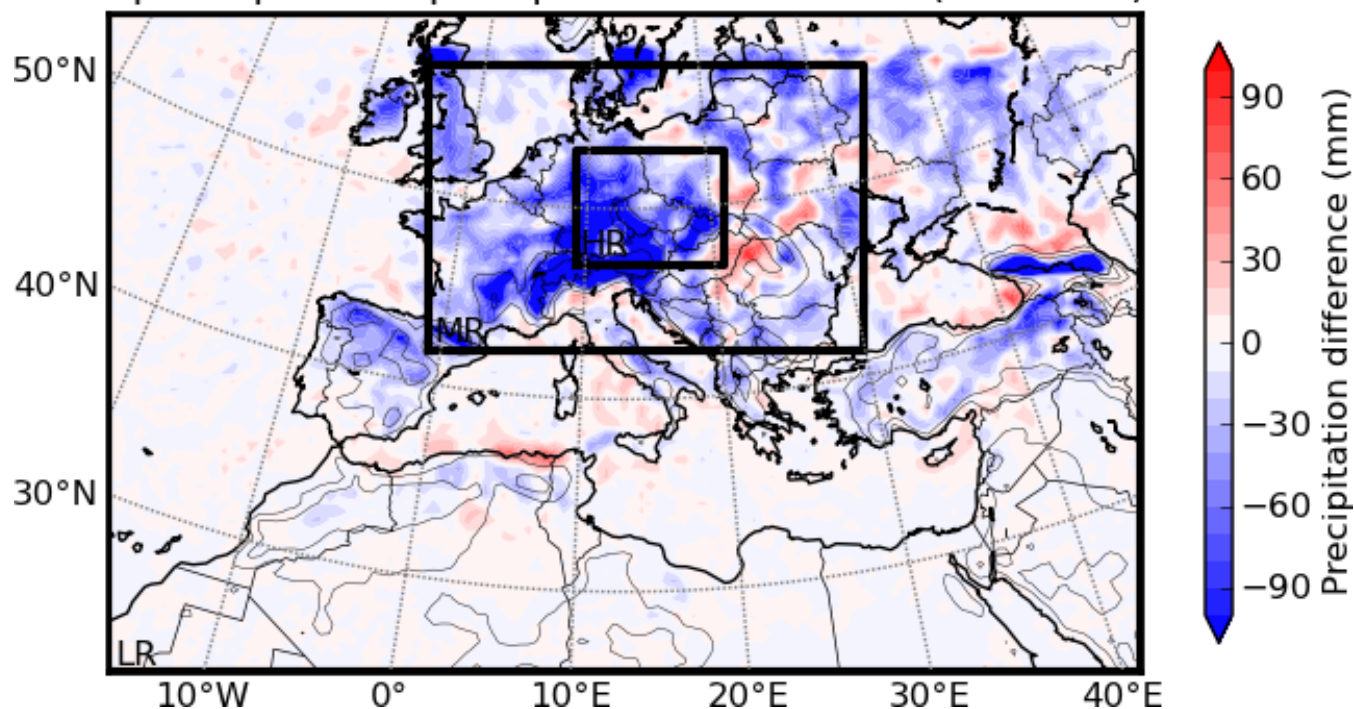


**Figure 2.** Differences of convective precipitation between the MAX and the MIN simulations. The whole map is the LR simulation domain, the medium black box is the intermediate domain MR, and the small box is the HR domain.

differences of aerosol concentrations between the two simulations ensure that aerosol indirect effects are strong enough to emerge from the potential noise between the MAX and the MIN simulations.

Another set of MIN and MAX simulations has been performed at a resolution where convection is resolved (3.3 km) and on a smaller domain (HR domain) as seen in Figure 2. An intermediate set of simulations was used to perform one-way nesting between the LR and the HR simulations, ensuring that the LR simulations force the HR simulations at their boundaries. These intermediate simulations were done at 16.6 km of resolution in an intermediate domain (see Fig.2) and with the same configuration as the LR simulations. In these conditions, each grid cell of the LR domain corresponds to exactly  $15 \times 15$  grid cells of the HR domain. The HR simulations have been performed without activating any convection scheme, since horizontal resolution (3.3 km) is sufficient to resolve convection processes, which is the only difference in model configuration between the LR simulations and the HR simulations.

### 2.3 Temperature-precipitation bin method

The simulation domain covers the Euro-Mediterranean region as displayed in Figure 2. This figure also shows the difference of accumulated convective precipitation over the period of study between the MAX and the MIN simulations. It shows that



most of the negative signal is concentrated over land regions where precipitation are more intense in this period of the year (Da Silva et al., 2018). The following analysis of convective precipitation reduction in the MAX simulation is conducted over the HR domain. Indeed, location of the HR domain was chosen because of the high negative values of convective precipitation differences between the MAX and the MIN simulations in this area and because it is far away from oceanic areas where flux imbalance with the non-coupled oceanic surface may hinder interpretation as discussed in Da Silva et al. (2018). Because of the short duration of our simulations, temperature at first vertical grid level and convective precipitation hourly time series were collected for all grid points of the WRF model that were inside the HR domain and then concatenated. To avoid snow precipitation we selected only the events with daily mean temperatures warmer than 5°C.

The method used to scale precipitation with temperature is similar to the one used by Hardwick et al. (2010). Temperature has a diurnal variation and may be impacted by precipitation events. Since for each precipitation event we want the corresponding temperature that represents the air mass, the daily averaged temperature is used. We select hours with strictly positive precipitation amount in both the MIN and MAX time series and place the pairs of daily mean temperatures and hourly precipitation into 8 bins of 5896 samples according to the daily temperatures. In each bin the 50<sup>th</sup> percentile of daily mean temperature, the 50<sup>th</sup> percentile of precipitation and the 95<sup>th</sup> percentile of precipitation are used for our analysis.

We focus on the contributions of precipitation efficiency, surface water vapor mixing ratio, and maximum vertical wind speed to the difference of convective precipitation scaling with temperature between the MAX and the MIN simulations. Precipitation efficiency is calculated using hourly output variables of WRF, and following the parameterization of Kain (2004) implemented in the model in which precipitation efficiency is a decreasing function of cloud base height and vertical wind shear. Because model output frequency is lower than the typical convective characteristic time, we expect large uncertainties. For the LR simulations, the maximum vertical wind speed is calculated using the square root of Surface Based Convective Available Potential Energy (SBCAPE) which is most representative of convective vertical motions than the resolved vertical velocity. These three variables are computed one hour before the convective precipitation occurrence to better represent the air inside the updraft of the convective cell rather than the air inside its downdraft.

The contribution of each variable to the change of precipitation between the MAX and MIN simulations is computed for both median and extreme precipitation events which are defined as following. Median events are all events where precipitation is between the 40<sup>th</sup> and the 60<sup>th</sup> percentile in at least one of the simulations (MIN or MAX). Extreme events are all events beyond the 90<sup>th</sup> percentile in at least one of the simulations (MIN or MAX). Median and extreme events are sorted as a function of the corresponding daily mean temperature and placed in 8 bins with the same number of events per bin. For median or extreme precipitation, the median of daily mean temperature is paired with each of the 4 variables (precipitation, precipitation efficiency, surface water vapor mixing ratio and maximum vertical wind speed along the atmospheric column) in the MIN and the MAX simulations.





### 3 Results

#### 3.1 Sensitivity of temperature-precipitation scaling to change in aerosol loads

Figure 3 displays the 50<sup>th</sup> (a, c) and 95<sup>th</sup> (b, d) percentiles of hourly convective (a, b) and total (c, d) precipitation as a function of daily mean temperature at the surface for both the MIN (magenta) and MAX (blue) simulations. Median convective precipitation follow a nearly CC-scaling in our LR simulations. However, there is a negative slope when considering total precipitation. It is therefore not surprising to find sub-CC scaling for total precipitation in the HR simulations (figure 4a). Lower slopes for median total precipitation are consistent with the study of Hardwick et al. (2010) in Australia.

Regarding convective precipitation extremes, a nearly CC-scaling appears in the LR simulation. Using in-situ measurements in Switzerland, Molnar et al. (2015) found a scaling of  $8.9\%.\text{°C}^{-1}$  of hourly convective precipitation as a function of daily mean temperature. Lower but similar slopes are obtained in our study with a value of  $6.1\%.\text{°C}^{-1}$  for the LR MIN simulation and a value of  $8.6\%.\text{°C}^{-1}$  in the LR MAX simulation. Berg and Haerter (2013) and Loriaux et al. (2013) showed that the scaling between total extreme precipitation and daily mean temperature could be super-CC because of the distribution of convective and stratiform precipitation with respect to daily mean temperature. Convective precipitation are generally more intense and occur at higher temperatures. Supposing that both convective and stratiform precipitation follow a CC-scaling, they argued that total precipitation will display a super-CC scaling for temperatures corresponding to the transition between stratiform and convective precipitation. Such an effect does not appear in our study since we can observe a slight sub-CC scaling for total extreme precipitation. The scaling of total extreme precipitation is therefore different from the hook shape found in the Drobinski et al. (2018) study in the Mediterranean area. As expected (Li et al., 2011), precipitation extremes are increased in the HR simulations with respect to the LR simulations. However the slopes of the HR simulations are rather similar to the slopes of total precipitation in the LR simulations.

Differences between the MAX and the MIN simulations are similar for both extremes and medians in HR and LR simulations. We find that convective precipitation are reduced in the MAX simulation but only at low temperatures. This temperature dependency slightly changes the scaling between the MAX and the MIN simulations, with higher slopes in the MAX simulation (around  $8.5\%.\text{°C}^{-1}$  in LR) compared to the MIN simulation (around  $6.2\%.\text{°C}^{-1}$  in LR). The fact that indirect effects of aerosols are weaker at high temperatures is probably due to the lower occurrence of clouds in these conditions. Figure 5 shows COD calculated as in Da Silva et al. (2018), as a function of daily mean temperature for both the MIN and MAX simulations for low and high resolutions. It confirms the weaker occurrence of clouds at high temperatures in our simulations, which results in weak differences in COD between the MAX and the MIN simulations for low and high resolution. On the contrary, clouds are numerous at low temperatures and create important differences of COD between the MAX and the MIN simulations which maximize indirect effects of aerosols. In their study of the impact of the microphysical scheme on the scaling of precipitation extremes with temperature, Singh and O’Gorman (2014) have also shown that the main effect occurs at low temperatures. They attributed the change of slope at low temperatures to a change of hydrometeor fall speed, parameterized differently depending on the microphysical scheme. In our case, convective precipitation are diagnosed with the same convective scheme in the MAX and MIN simulations, which neither takes into account aerosol concentrations nor rain fall speed. Such microphysical effect

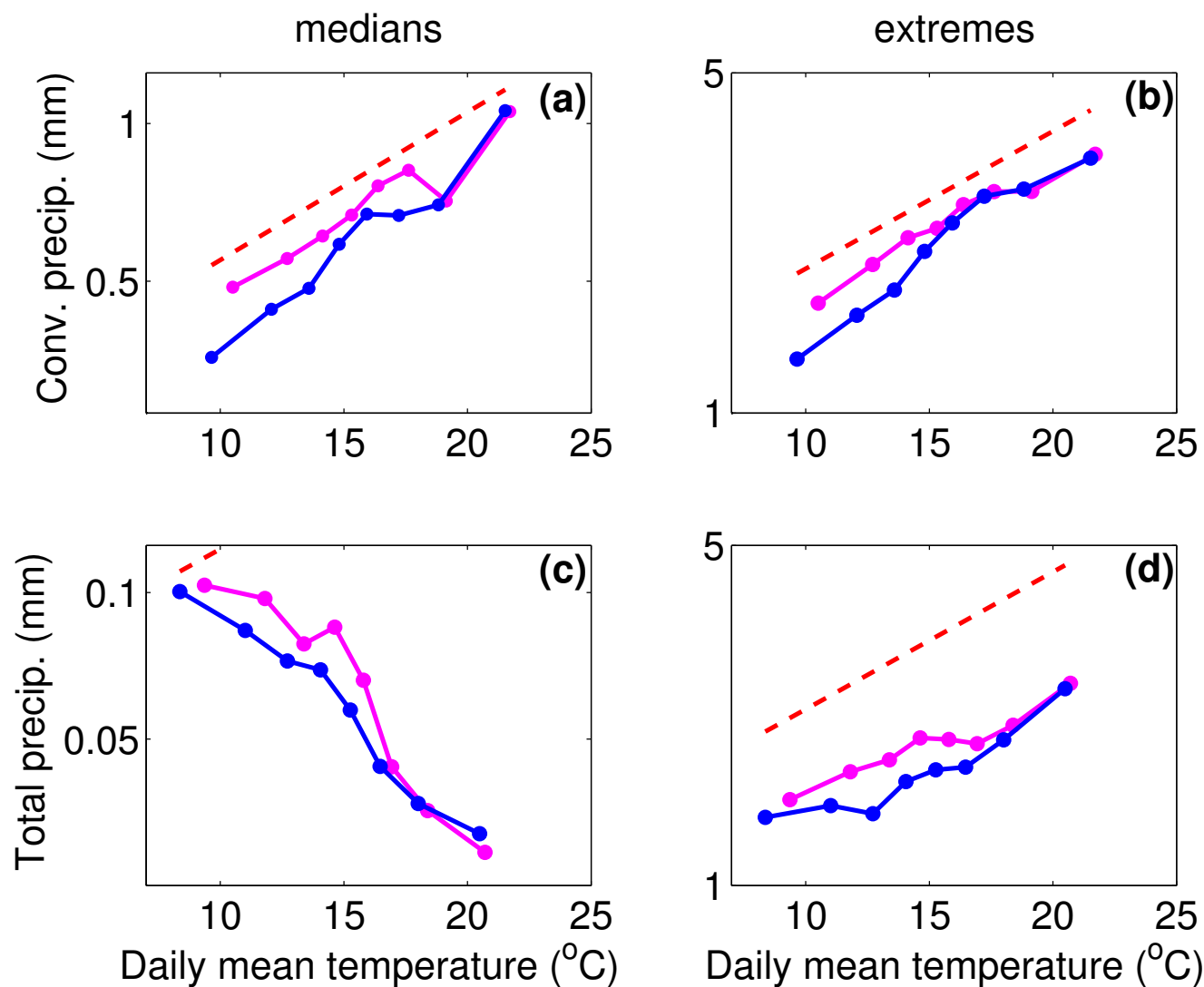


**Figure 3.** Hourly convective (a, b) and total (c, d) precipitation as a function of daily mean temperature at the surface for median (a, c) and extreme (95<sup>th</sup> percentile, b, d) precipitation and for both the LR MIN (magenta) and LR MAX (blue) simulations. The dashed red line indicates the CC-slope calculated using the August-Magnus-Roche approximation for saturated vapor pressure (Alduchov and Eskridge, 1996).



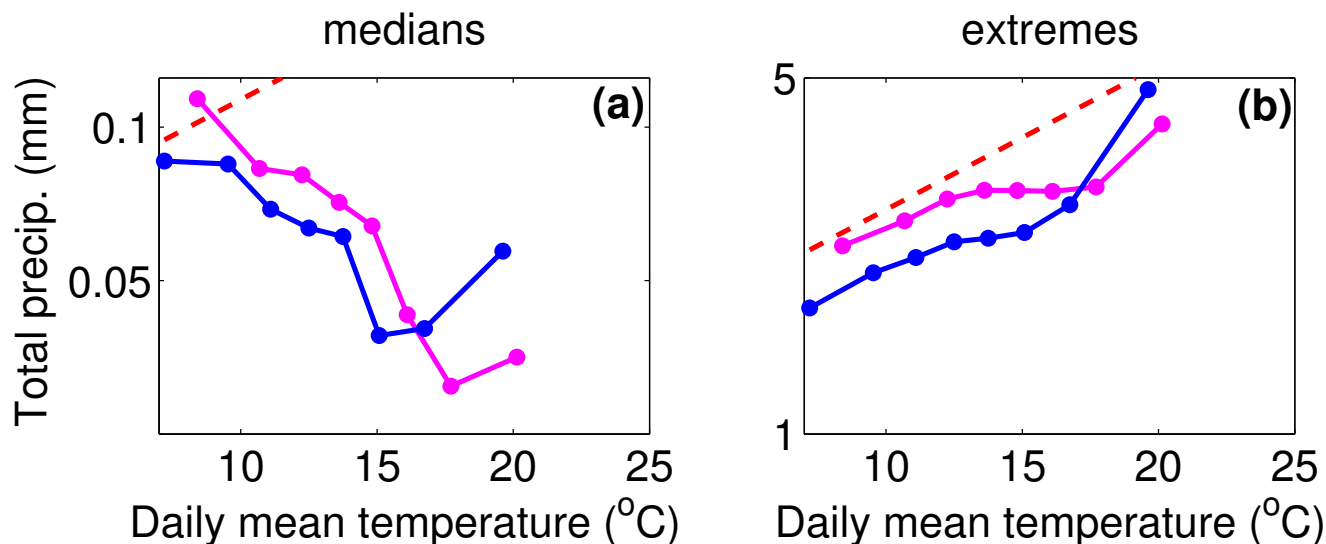


**Figure 4.** Hourly total precipitation as a function of daily mean temperature at the surface for median (a) and extreme (95<sup>th</sup> percentile, b) precipitation and for both the HR MIN (magenta) and HR MAX (blue) simulations. The dashed red line indicates the CC-slope calculated using the August-Magnus-Roche approximation for saturated vapor pressure.

is therefore impossible in our configuration. We believe that the inhibition of convective precipitation is mainly due to the processes described in Da Silva et al. (2018), i.e. a stabilisation of the atmosphere and a reduction of precipitable water in the polluted simulations.

### 3.2 Process analysis

- 5 To analyse the reduction of convective precipitation at low temperatures we consider that precipitation can be approximately described by the following equation:

$$Pr \propto \epsilon \times Q \times W \quad (2)$$

with  $\epsilon$  corresponding to the precipitation efficiency,  $Q$  the water vapor mixing ratio at the surface and  $W$  the maximum vertical wind speed. This description is mostly valid for convective precipitation which result from a parcel that raises from the surface.

- 10 Assuming the small changes of precipitation that we observe between the MAX and the MIN simulations, one can write :

$$\frac{Pr_{MAX} - Pr_{MIN}}{Pr_{MIN}} = \frac{\epsilon_{MAX} - \epsilon_{MIN}}{\epsilon_{MIN}} + \frac{Q_{MAX} - Q_{MIN}}{Q_{MIN}} + \frac{W_{MAX} - W_{MIN}}{W_{MIN}} \quad (3)$$

Figure 6 displays relative changes in convective precipitation vertical wind speed, precipitation efficiency, and surface water vapor mixing ratio between the LR MAX and LR MIN simulations for median and extreme precipitation. As expected from figure 5, the decrease of convective precipitation in the MAX simulation with respect to the MIN simulation tends to be weaker

- 15 with increasing temperatures, from  $-25\%$  at  $10^\circ\text{C}$  until almost  $0\%$  at  $22^\circ\text{C}$ . Among the three factors that may impact the

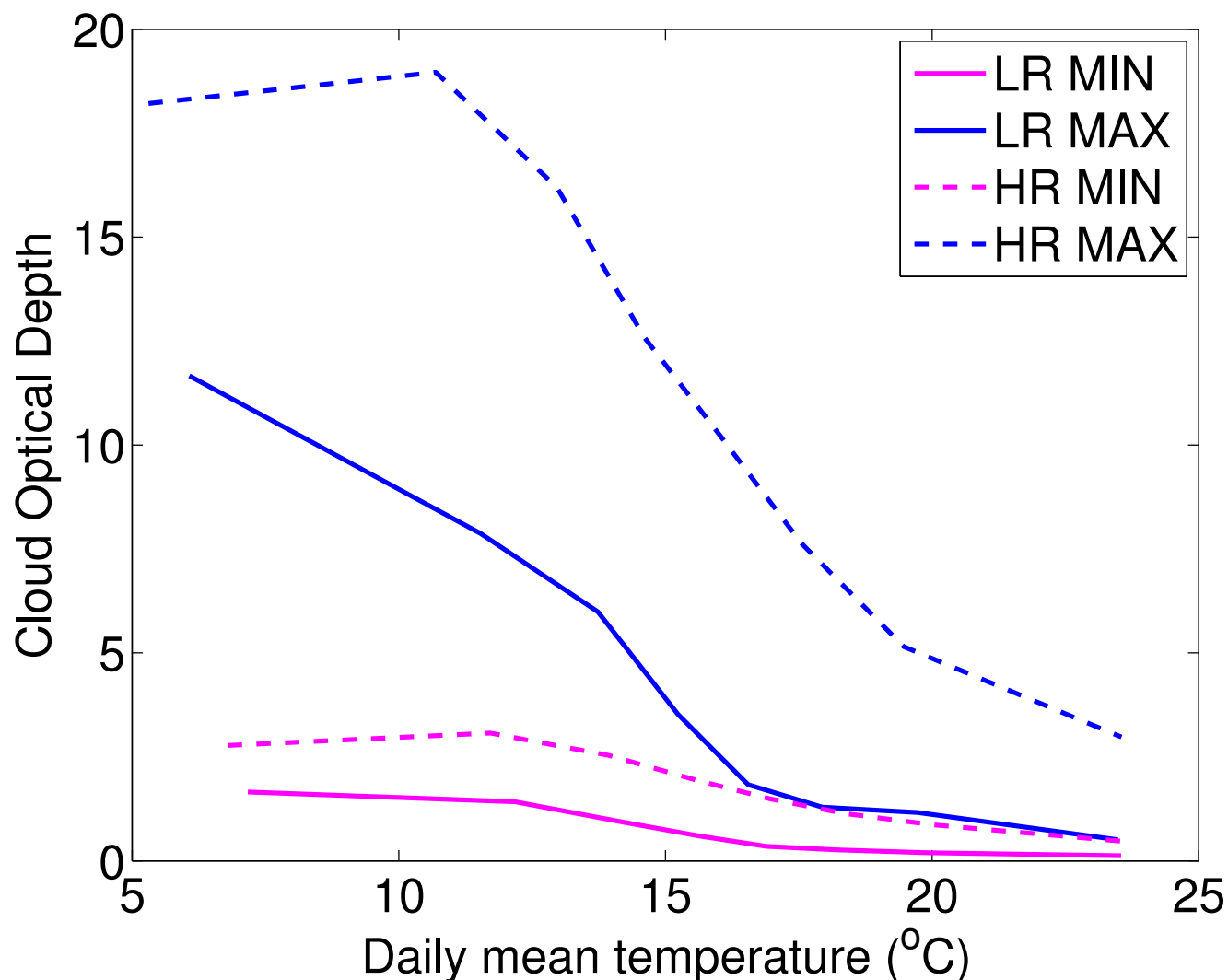


**Figure 5.** Hourly COD as a function of daily mean temperature for the LR MIN (full magenta line), LR MAX (dashed blue line), HR MIN (dashed magenta line) and HR MAX (dashed blue line) simulations.

precipitation intensity, the vertical velocity seems to explain much of the reduction of convective precipitation. Indeed, among the 25% of precipitation reduction at low temperatures, around 15% are attributable to the weakening of vertical velocity in the MAX simulation. It is also striking in Fig. 6 that the variations of the difference of vertical velocity and of convective precipitation with temperature are perfectly similar, with stronger reductions for low temperature than for higher ones, while both precipitation efficiency and surface water vapor mixing ratio display insignificant or erratic variations with temperature. Indeed, the high variations of precipitation efficiency differences with temperature for precipitation extremes may not reflect a physical process but only the difficulty in retrieving precipitation efficiency from hourly outputs.

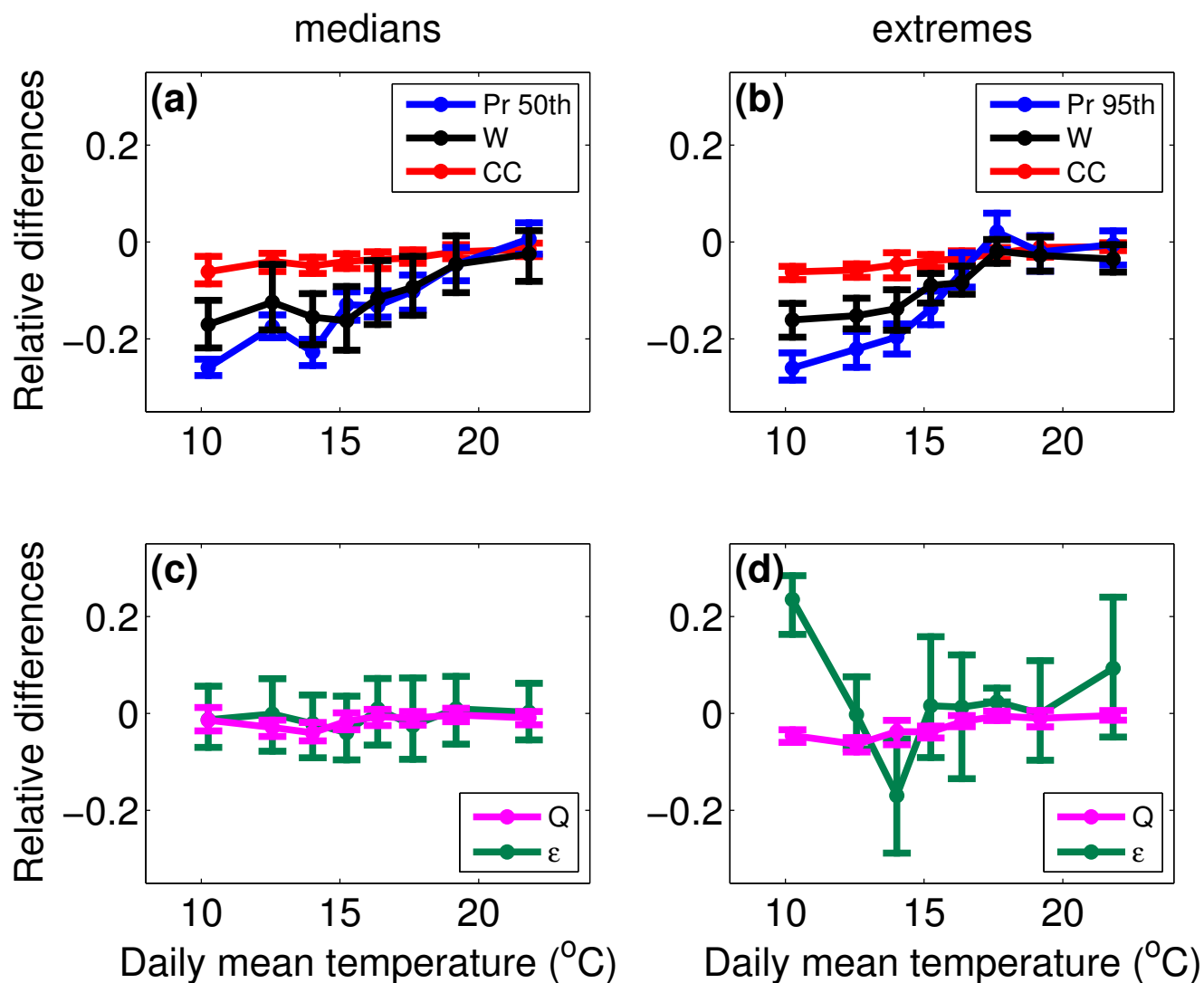


**Figure 6.** Relative differences between LR MAX and LR MIN simulations of convective precipitation (blue, a and b), vertical velocity (black, a and b), surface water vapor mixing ratio (magenta, c and d), precipitation efficiency (green, c and d) for median (a and c) and extreme (b and d) convective precipitation events as a function of the mean between the MIN and MAX daily mean temperature. The change expected according to the Clausius-Clapeyron law is displayed in red (a and b).



The fact that vertical velocity drives the changes in convective precipitation explains why the CC-scaling is completely inaccurate for predicting changes in convective precipitation by indirect effects. In fact, even the differences of surface water vapor mixing ratio between the MAX and MIN simulations do not exactly follow a CC-scaling due to increased relative humidity in the MAX simulation: while the CC law prediction is around  $-4\%$ , the reduction of surface water vapor mixing ratio in the MAX simulation is often less important. One would expect that the sub-CC scaling of surface water vapor mixing ratio differences would result in a sub-CC scaling of convective precipitation differences but it is actually the reverse (super-CC scaling) because of stronger changes in vertical velocity.

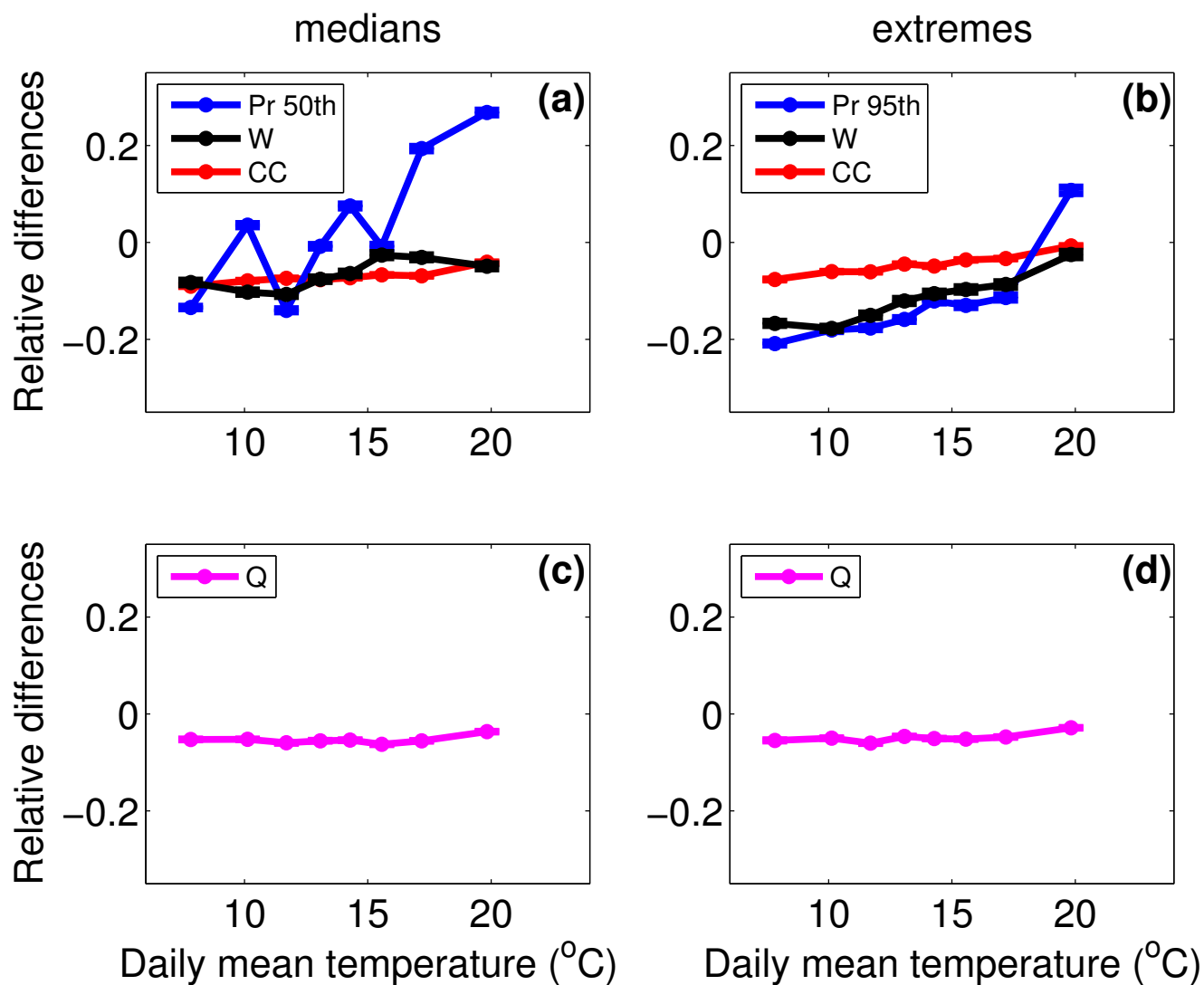
Results are similar for both extreme and median precipitation except for precipitation efficiency differences which displays small variations for median precipitation and erratic variations for extreme precipitation which may not have a physical meaning.

Figure 7 is the same as figure 6 but for the HR total precipitation. We did not evaluate precipitation efficiency, since it is not parameterized for explicitly resolved precipitation. Although the differences of vertical velocity and surface water vapor mixing ratio for median precipitation events have approximately the same behavior with temperature in the HR simulation with respect to the LR simulation, MAX-MIN differences of total HR precipitation are stronger than the differences of LR convective precipitation. Such positive bias compared to LR convective precipitation differences may be expected since Da Silva et al. (2018) showed that stratiform precipitation are increased in the MAX simulation. Extreme precipitation are mostly of convective nature, therefore differences of extreme total precipitation in the HR simulation are similar to the convective ones in the LR simulation and scale well with the differences of maximum vertical velocities.

### 3.3 Contributions of humidity and temperature to stability changes

As mentioned in section 2.3, vertical velocity is calculated as the square root of SBCAPE. As seen in Fig.1, SBCAPE may be affected by both surface temperature and surface humidity. SBCAPE is calculated using the entire profile of temperature and relative humidity (RH). In this line, we want to quantify the contribution of both the temperature and RH profile changes in the decrease of SBCAPE in the MAX simulation. For that purpose we have substituted the vertical profile of temperature in the MIN simulation, by the vertical profile of temperature from the MAX simulation, and we have calculated two additional SBCAPEs, i.e.  $SBCAPE_T$  (resp.  $SBCAPE_{RH}$ ) calculated with the temperature profile from the MAX (resp. MIN) simulation and the relative humidity from the MIN (resp. MAX) simulation, as represented in Figure 8. Using the 4 SBCAPEs ( $SBCAPE_{MIN}$ ,  $SBCAPE_{MAX}$ ,  $SBCAPE_{RH}$  and  $SBCAPE_T$ ) we can compute relative differences ( $\Delta SBCAPE_{RH,1}$ ,  $\Delta SBCAPE_{RH,2}$ ,  $\Delta SBCAPE_{T,1}$ ,  $\Delta SBCAPE_{T,2}$ , and  $\Delta SBCAPE$ , see Fig. 8) and thus infer the contribution of temperature and RH vertical profiles in the change of SBCAPE between the MAX and the MIN simulations.

Figure 9 shows the total change of SBCAPE between the MAX and MIN simulations ( $\Delta SBCAPE$ ), the RH contribution ( $\Delta SBCAPE_{RH} = \frac{\Delta SBCAPE_{RH,1} + \Delta SBCAPE_{RH,2}}{2}$ ), and the temperature contribution ( $\Delta SBCAPE_T = \frac{\Delta SBCAPE_{T,1} + \Delta SBCAPE_{T,2}}{2}$ ) as a function of daily mean temperature for median and extreme precipitation events. The quantity SBCAPE is lower in the MAX simulation with respect to the MIN simulation, and  $\Delta SBCAPE$  is more negative at low temperatures ( $-30\%$ ) than at high temperatures (almost  $0\%$ ). However one can see that  $\Delta SBCAPE_T$  and  $\Delta SBCAPE_{RH}$  have opposite signs. Indeed, the



**Figure 7.** Relative differences between HR MAX and HR MIN simulations of total precipitation (blue) and vertical velocity (black, a and b) and surface water vapor mixing ratio ( $Q$ , magenta, c and d) for median (a and c) and extreme (b and d) precipitation events as a function of the mean between the MIN and MAX daily mean temperature. The change expected according to the Clausius-Clapeyron law is displayed in red (a and b).

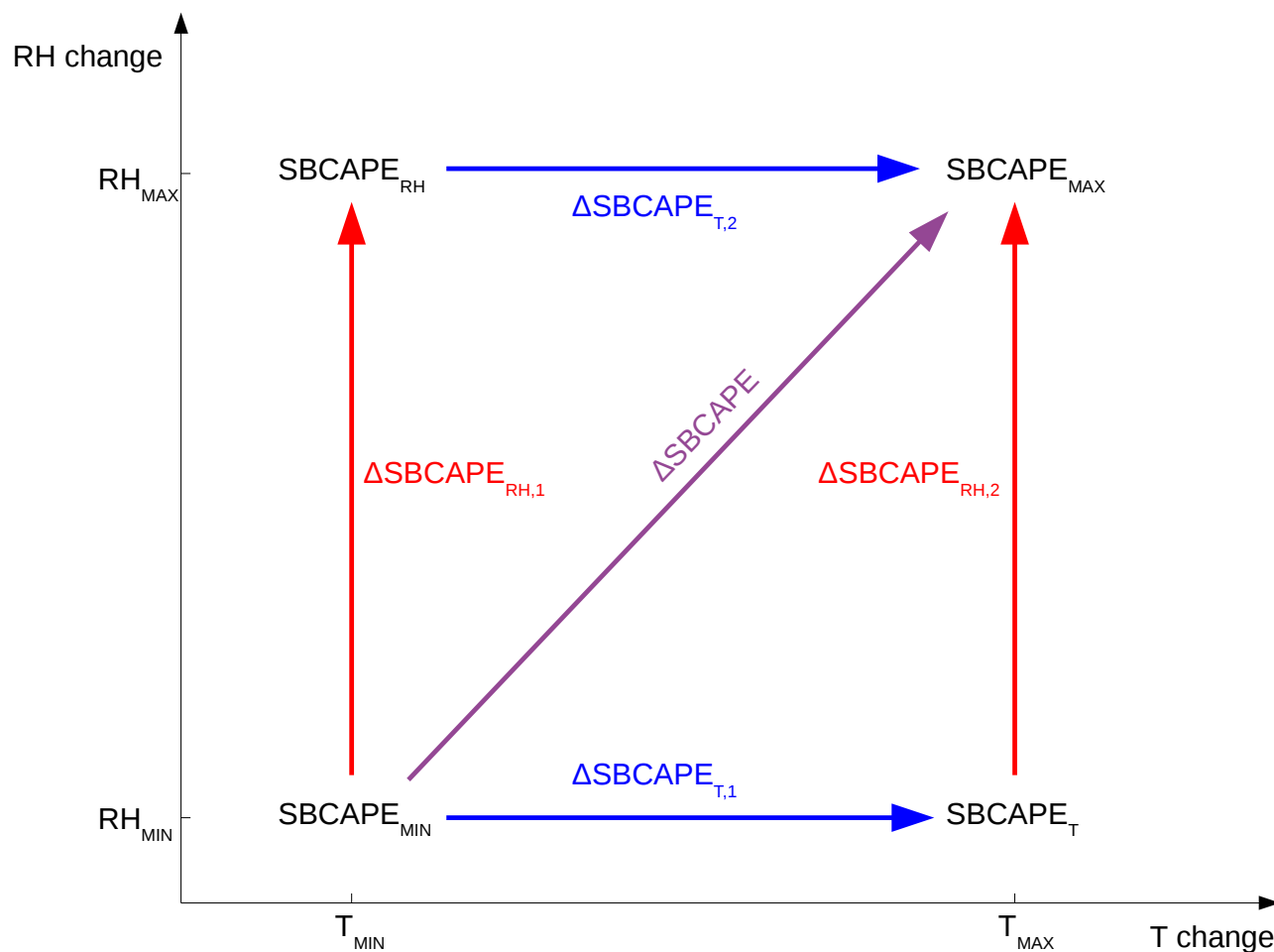


**Figure 8.** Schematic of the 2 possible SBCAPE differences that permit to evaluate the contribution of the vertical profile of temperature ( $\Delta SBCAPE_{T,1}$  and  $\Delta SBCAPE_{T,2}$ ) and the contribution of the vertical humidity profile ( $\Delta SBCAPE_{RH,1}$  and  $\Delta SBCAPE_{RH,2}$ ) to the change of total SBCAPE between the MAX and the MIN simulations ( $\Delta SBCAPE$ ).



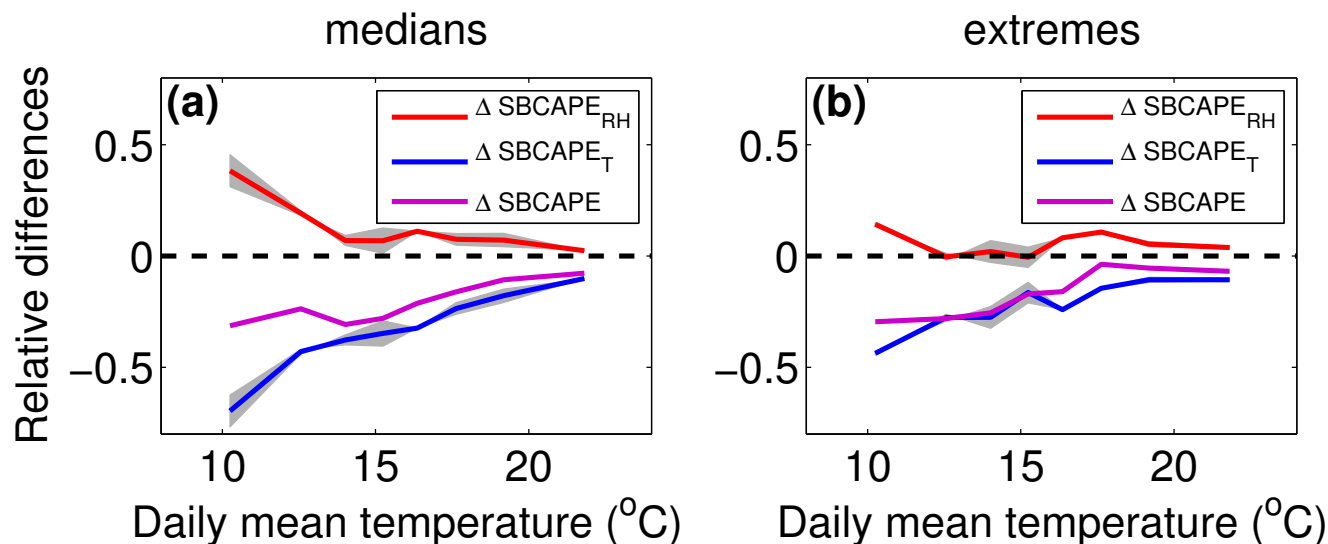


**Figure 9.** Relative differences of SBCAPEs for median (a) and extreme (b) convective precipitation events of the relative difference between the LR MAX and the LR MIN simulations (magenta,  $\Delta\text{SBCAPE}$ ). The temperature contribution ( $\Delta\text{SBCAPE}_T$ ) is displayed in blue and the relative humidity contribution ( $\Delta\text{SBCAPE}_{RH}$ ) in red.

RH contribution is positive and decreases from about +40% at 10°C to about 0% at 22°C for median precipitation events. The fact that this contribution is positive is not a surprise since we have seen in Fig. 6 that the surface RH is higher in the MAX simulation. We can see that this apparently weak increase of RH in the MAX simulation has a strong effect on the SBCAPE at low temperatures. However the main contribution is negative and comes from the differences of vertical temperature profiles: values are ranging between -70% at low temperatures and -15% at high temperatures. Moreover, one can see similar variations of  $\Delta\text{SBCAPE}$  and  $\Delta\text{SBCAPE}_T$  with temperature.

Figure 10 is the same as figure 9 but for the HR simulations and total precipitation. The quantity  $\Delta\text{SBCAPE}$  is larger in the HR simulation with values that exceed -50% for a wide range of low temperatures in both median and extreme precipitation. These large values of  $\Delta\text{SBCAPE}$  result in small negative differences of maximum vertical wind speed that do not exceed -10% and are not correlated with total precipitation differences for median total precipitation events (see figure 7) because of the coexistence of convective and stratiform events. Otherwise contributions are similar to those of the LR simulations with mainly a positive contribution of RH and a strongly negative contribution from the temperature vertical profile.

The quantity SBCAPE is a non-linear function of the temperature and humidity profiles. Therefore, the change  $\Delta\text{SBCAPE}_{T,1}$  is different from the change  $\Delta\text{SBCAPE}_{T,2}$ . Similarly, the change  $\Delta\text{SBCAPE}_{RH,1}$  is different from the change  $\Delta\text{SBCAPE}_{RH,2}$ . The quantities  $\Delta\text{SBCAPE}_{T,1}$  and  $\Delta\text{SBCAPE}_{T,2}$  (resp.  $\Delta\text{SBCAPE}_{RH,1}$  and  $\Delta\text{SBCAPE}_{RH,2}$ ) delimit a grey area in Fig. 9 that represents the uncertainty (relative to the non-linearity of SBCAPE) of the temperature (resp. RH) contribution. One can see that the effects of SBCAPE non-linearity are generally lower than

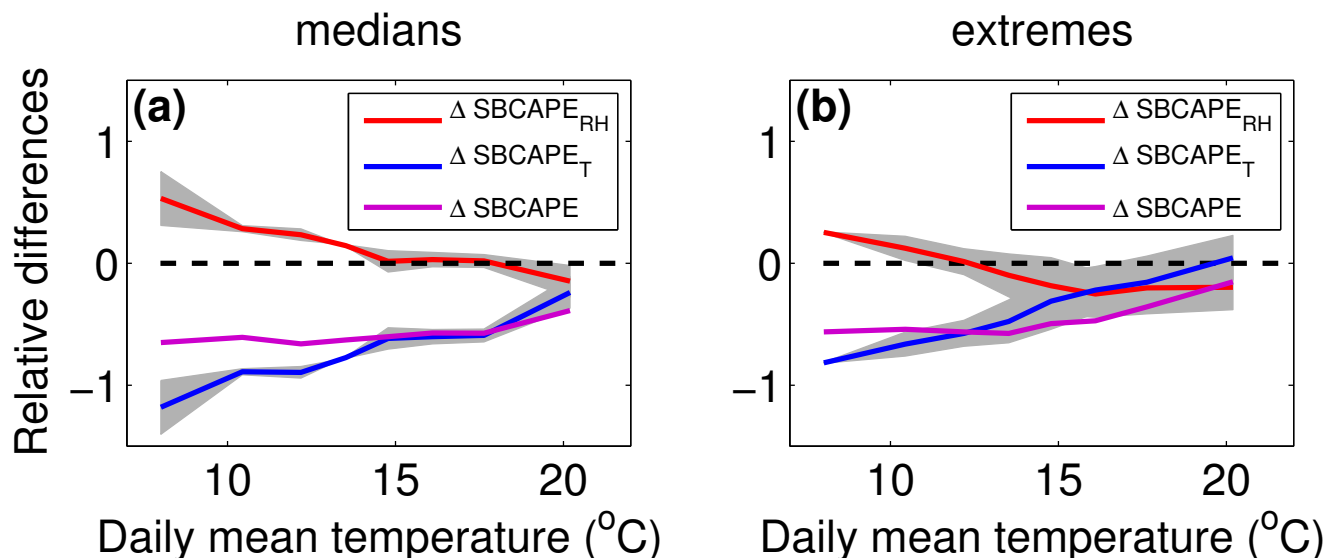


**Figure 10.** Relative differences of SBCAPEs for median (on the left) and extreme (on the right) precipitation events of the relative difference between the HR MAX and the HR MIN simulations (magenta,  $\Delta\text{SBCAPE}$ ). The temperature vertical profile contribution ( $\Delta\text{SBCAPE}_T$ ) is displayed in blue and the relative humidity vertical profile contribution ( $\Delta\text{SBCAPE}_{RH}$ ) in red.

the difference between each contribution. Where the grey areas do not intersect, i.e. in almost the entire temperature range for median precipitation, and for the cooler part of the distribution for extreme precipitation, comparison of  $\Delta\text{SBCAPE}_T$ ,  $\Delta\text{SBCAPE}_{RH}$  and  $\Delta\text{SBCAPE}$  strengthen the interpretation presented above: the negative value of  $\Delta\text{SBCAPE}$  can be attributed to temperature changes, partly buffered by RH changes.

- 5 However the vertical temperature profile can be changed in several ways, e.g. one can only change the vertical gradient of temperature or uniformly reduce the temperature on the vertical. In the first configuration the decrease of SBCAPE would be purely due to the increase of stability of the environment whereas in the second configuration the decrease of SBCAPE would be due to the surface air parcel temperature, more precisely to its reduced release of latent heat due to reduction of its initial water vapor content.
- 10 In this part, the temperature contribution is decomposed into two contributions, one from the vertical gradient of temperature and one from the surface temperature. The quantity SBCAPE can now be viewed as a function of three variables: the RH profile, the vertical temperature gradient and the surface temperature. As displayed in Fig. 11, for a given RH profile (from the MIN or the MAX simulation), we have substituted the vertical temperature gradient (resp. surface temperature) from the MIN simulation, by the vertical temperature gradient (resp. surface temperature) from the MAX simulation, and we have calculated
- 15 4 additional SBCAPEs using the 4 new mixed profiles. By calculating relative differences of SBCAPE, one can evaluate the contribution of the surface temperature ( $\Delta\text{SBCAPE}_{T_s} = \frac{1}{4} \sum_{i=1}^{i=4} \Delta\text{SBCAPE}_{T_s,i}$ ) and of the vertical gradient of temperature ( $\Delta\text{SBCAPE}_{\nabla_z T} = \frac{1}{4} \sum_{i=1}^{i=4} \Delta\text{SBCAPE}_{\nabla_z T,i}$ ).

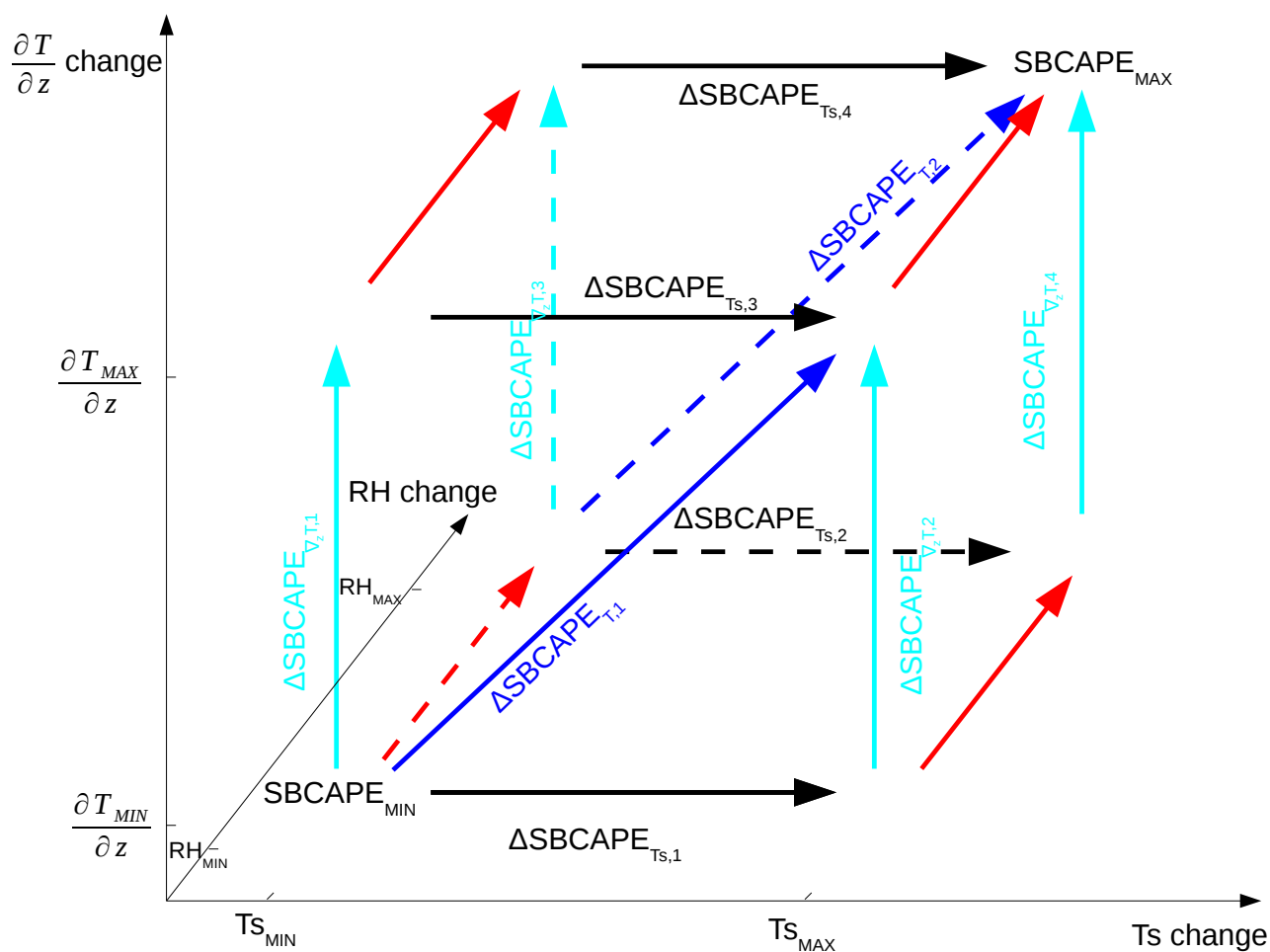


**Figure 11.** Schematic of the 4 possible SBCAPE differences that permit to evaluate the contribution of the vertical gradient of temperature ( $\Delta SBCAPE_{\nabla_z T,1}$ ,  $\Delta SBCAPE_{\nabla_z T,2}$ ,  $\Delta SBCAPE_{\nabla_z T,3}$ , and  $\Delta SBCAPE_{\nabla_z T,4}$ ) and the contribution of the surface temperature ( $\Delta SBCAPE_{Ts,1}$ ,  $\Delta SBCAPE_{Ts,2}$ ,  $\Delta SBCAPE_{Ts,3}$ , and  $\Delta SBCAPE_{Ts,4}$ ) to  $\Delta SBCAPE$ .

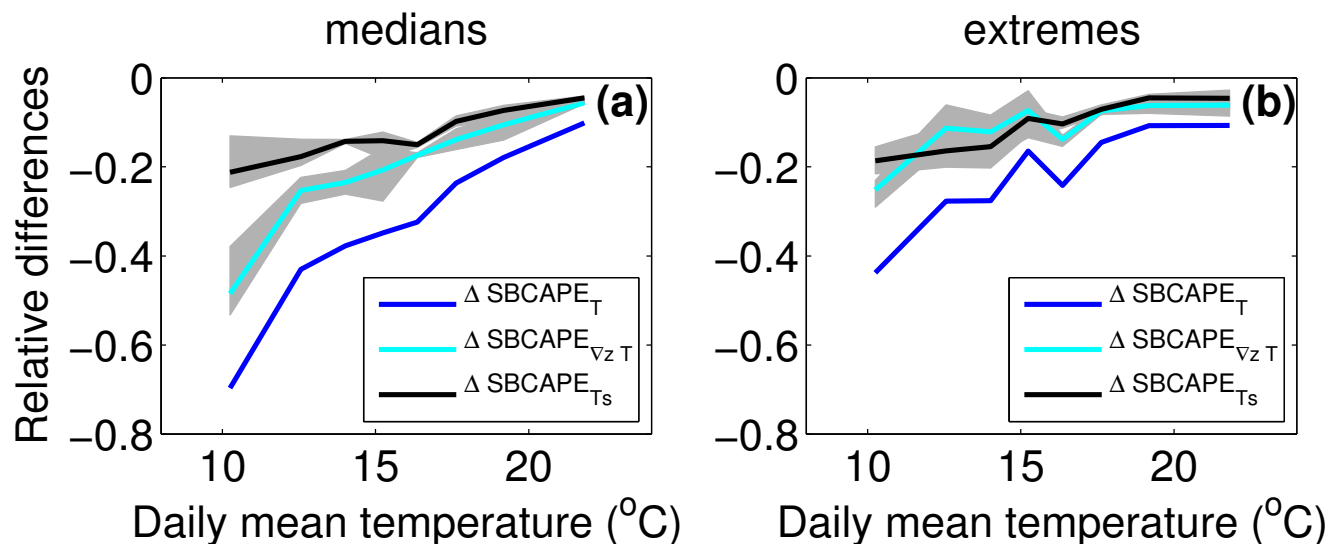


**Figure 12.** Relative differences of SBCAPEs for median (a) and extreme (b) convective precipitation events of the temperature contribution to the relative difference between the LR MAX and the LR MIN simulations (blue,  $\Delta\text{SBCAPE}_T$ ). The surface temperature contribution ( $\Delta\text{SBCAPE}_{T_s}$ ) is displayed in black and the temperature vertical gradient contribution ( $\Delta\text{SBCAPE}_{\nabla_z T}$ ) in cyan.

Figure 12 shows  $\Delta\text{SBCAPE}_{\nabla_z T}$ ,  $\Delta\text{SBCAPE}_{T_s}$  and  $\Delta\text{SBCAPE}_T$  (as in Fig. 8) as a function of daily mean temperature for the LR simulations. The contribution of the vertical gradient of temperature and the contribution of the surface temperature are both negative, indicating not only that the surface temperature is lower in the MAX simulation but also that this cooling is less important in the higher layers of the troposphere. Both processes tend to reduce the SBCAPE in the MAX simulation with respect to the MIN simulation. For median precipitation, the reduction of SBCAPE due to the vertical gradient of temperature (-10% at high temperatures to -50% at low temperatures) is more important than the reduction of SBCAPE due to the surface temperature (-10% at high temperatures to -20% at low temperatures). For extreme precipitation, contributions are similar and range between -20% at low temperatures to -5% at high temperatures.

A similar analysis in the HR simulations is displayed in figure 13. The results are very similar to those from the LR simulations with the exception that for extreme precipitation with low temperatures, the temperature gradient contribution is significantly larger than the surface temperature contribution.

The maximum and the minimum values of  $\Delta\text{SBCAPE}_{T_s,i}$  (resp.  $\Delta\text{SBCAPE}_{\nabla_z T,i}$ ) delimit a grey area in Figures 12 and 13 that represent the uncertainty related to the SBCAPE non-linearity. It shows that for both HR and LR simulations, contributions are clearly different at low temperatures for median precipitation events whereas the uncertainty ranges tend to overlap at high temperatures. For extreme events, the non-linearity of SBCAPE does not permit to distinguish the two contributions for the entire range of temperatures of the LR simulations. In the HR simulations, the non-linearity uncertainty is also too large at

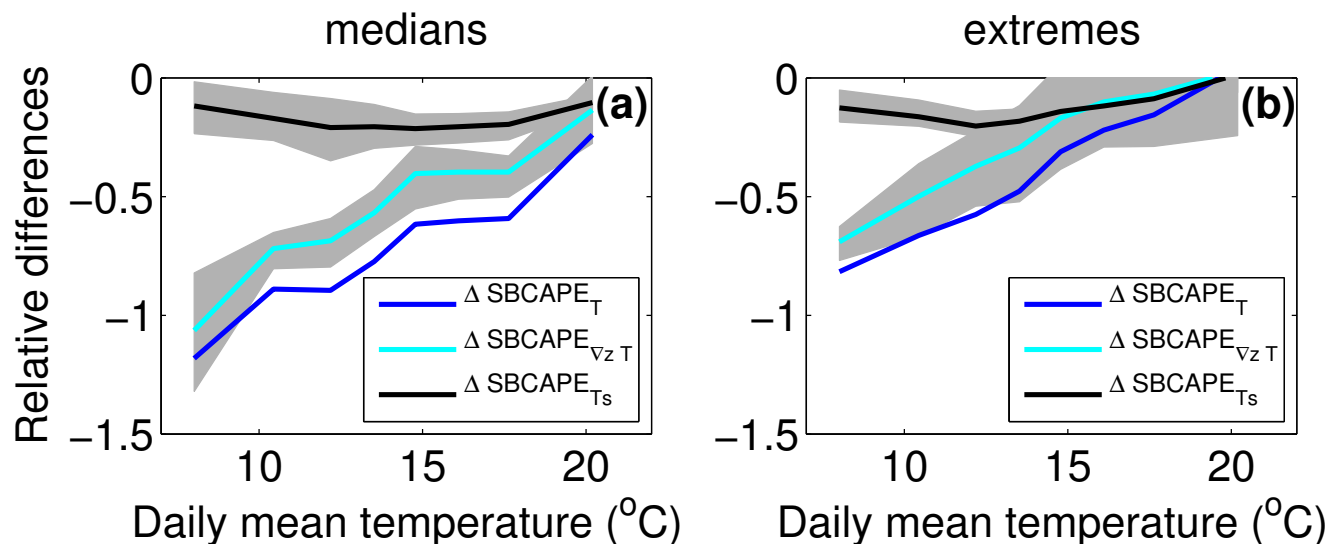


**Figure 13.** Relative differences of SBCAPEs for median (a) and extreme (b) precipitation events of the temperature contribution to the relative differences between the HR MAX and the HR MIN simulations (blue,  $\Delta\text{SBCAPE}_T$ ). The surface temperature contribution ( $\Delta\text{SBCAPE}_{T_s}$ ) is displayed in red and the temperature vertical gradient contribution ( $\Delta\text{SBCAPE}_{\nabla_z T}$ ) in blue.

high temperatures to differentiate the two contributions. However the contribution of the vertical gradient of temperature is significantly weaker than the contribution of the surface temperature at the lowest temperatures of the HR simulations.

#### 4 Conclusions

An evaluation of the processes involved in the reduction of convective precipitation by aerosol indirect effects is performed in the present study in the frame of the temperature-precipitation relationship. Figure 14 summarizes the various involved processes and their qualitative contribution (size of the arrows). The temperature-precipitation approach permits to show that aerosol indirect effects on convective precipitation are larger at low temperatures than at high temperatures because clouds are statically more frequent and optically thicker at cool temperatures in our area of interest. Da Silva et al. (2018) found that convective precipitation are weakened in polluted environment through reduced atmospheric instability and water availability. With a simple decomposition of the decrease of convective precipitation in the polluted simulation, we show that this decrease is dominated by differences in atmospheric stability rather than differences in the moisture content of air parcels (Fig. 14). Therefore, the reduction of convective precipitation in the polluted simulation does not follow the Clausius-Clapeyron law: the simulated reduction in convective precipitation in a polluted environment compared to a pristine environment as determined in our simulations is actually stronger than the Clausius-Clapeyron scaling.

Using the SBCAPE parameter as a measure of the atmospheric stability, we perform an in-depth analysis that estimates the contribution of each variable to the weakening of convective updrafts in the polluted simulation. Quantifying uncertainties



related to the non-linearity of the SBCAPE is essential to correctly attribute the contribution of each variable to the stability modifications. Our method gives a first estimation of these uncertainties and shows that they are small enough to assess the following conclusions. The weakening of vertical velocity in convective updrafts is essentially explained by the stabilisation of the vertical profile of temperature, which is partly compensated by an increase of relative humidity in the polluted simulation (Fig. 14). The modification of the vertical temperature gradient, due to a stronger cooling in the boundary layer than in the free troposphere in the polluted simulation, is the most important contribution for median precipitation events whereas for extreme precipitation it is of similar magnitude as the contribution of the surface temperature decrease. Our simulations performed at high resolution are consistent with these results even though their interpretation is made more difficult by the fact that convective and stratiform precipitation are melted together while having opposite responses to aerosol indirect effects (as seen in Da Silva et al., 2018).

*Data availability.* The WRF simulations used in this study can be obtained in the MISTRAL database website (registration required) at <http://mistrals.sedoo.fr/?editDatsId=1503> or upon request to the authors.

*Author contributions.* The authors designed the numerical experiments. Nicolas Da Silva and Sylvain Mailler performed the simulations. Nicolas Da Silva prepared the manuscript with contributions from all co-authors.

*Competing interests.* The authors declare that they have no conflict of interest.

*Acknowledgements.* This work is a contribution to the HyMeX program (HYdrological cycle in the Mediterranean EXperiment) through INSU-MISTRALS support.



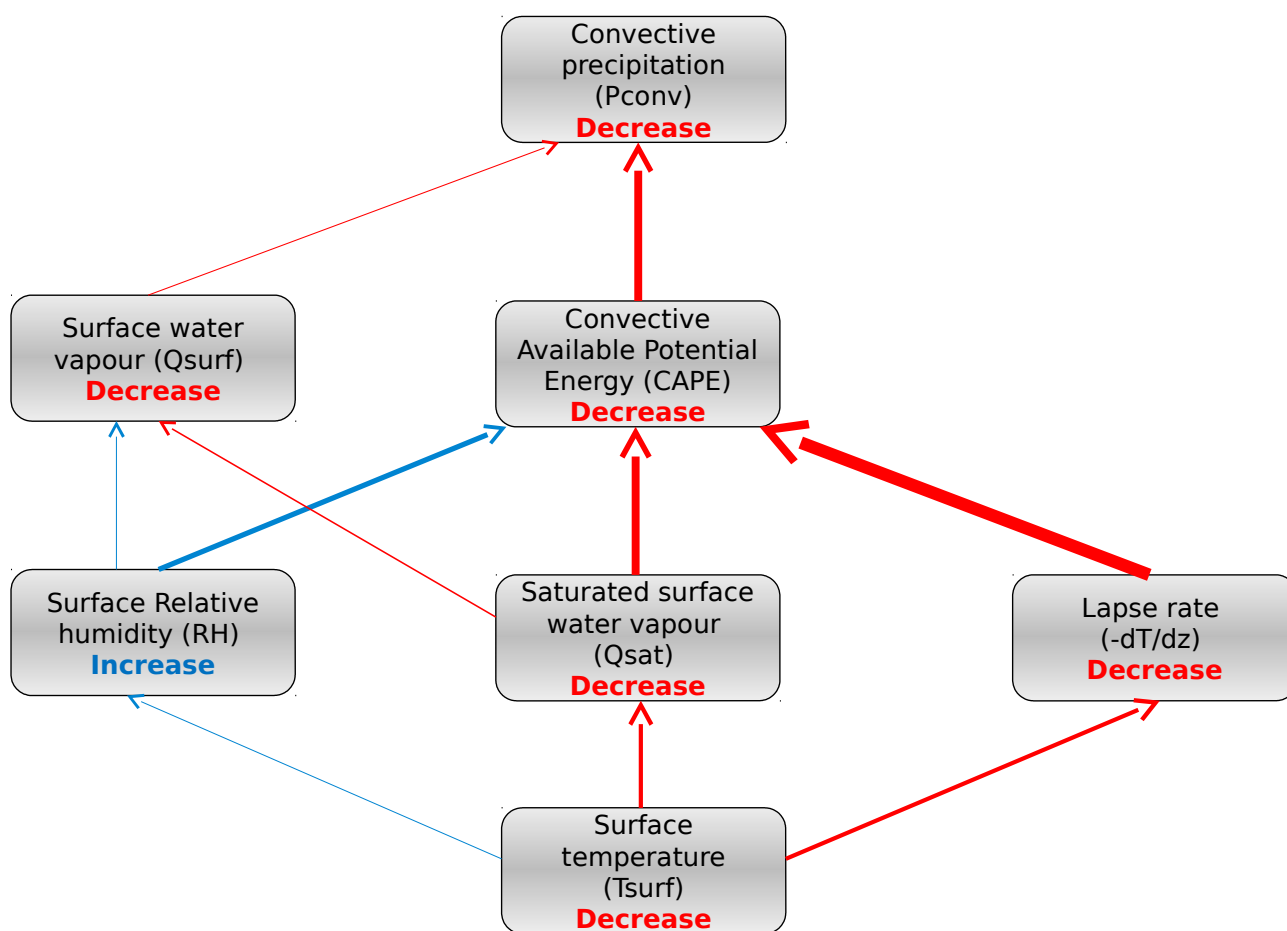


**Figure 14.** Detailed schematic summary of the causal sequence that links the decrease of surface temperature to the decrease of convective precipitation in a polluted environment. The size of arrows gives a qualitative estimation of the contributions of each processes.



## References

- Adler, R. F., Gu, G., Wang, J., Huffman, G. J., Curtis, S., and Bolvin, D.: Relationships between global precipitation and surface temperature on interannual and longer timescales (1979–2006), *Journal of Geophysical Research: Atmospheres*, 113, <https://doi.org/10.1029/2008JD010536>, 2008.
- 5 Albrecht, B.: Aerosols, cloud microphysics, and fractional cloudiness, *Science*, 245, 1227–1230, <https://doi.org/10.1126/science.245.4923.1227>, 1989.
- Alduchov, O. A. and Eskridge, R. E.: Improved Magnus Form Approximation of Saturation Vapor Pressure, *Journal of Applied Meteorology*, 35, 601–609, [https://doi.org/10.1175/1520-0450\(1996\)035<0601:IMFAOS>2.0.CO;2](https://doi.org/10.1175/1520-0450(1996)035<0601:IMFAOS>2.0.CO;2), 1996.
- Allen, M. R. and Ingram, W. J.: Constraints on future changes in climate and the hydrologic cycle, *Nature*, 419, 224, <https://doi.org/10.1038/nature01092>, 2002.
- 10 Berg, P. and Haerter, J.: Unexpected increase in precipitation intensity with temperature — A result of mixing of precipitation types?, *Atmospheric Research*, 119, 56 – 61, <https://doi.org/https://doi.org/10.1016/j.atmosres.2011.05.012>, 2013.
- Boer, G. J.: Climate change and the regulation of the surface moisture and energy budgets, *Climate Dynamics*, 8, 225–239, <https://doi.org/10.1007/BF00198617>, 1993.
- 15 Bollasina, M. A., Ming, Y., and Ramaswamy, V.: Anthropogenic Aerosols and the Weakening of the South Asian Summer Monsoon, *Science*, 334, 502–505, <https://doi.org/10.1126>, 2011.
- Da Silva, N., Mailler, S., and Drobinski, P.: Aerosol indirect effects on summer precipitation in a regional climate model for the Euro-Mediterranean region, *Annales Geophysicae*, 36, 321–335, <https://doi.org/10.5194/angeo-36-321-2018>, 2018.
- Drobinski, P., Ducrocq, V., Alpert, P., Anagnostou, E., Béranger, K., Borga, M., Braud, I., Chanzy, A., Davolio, S., Delrieu, G., Estournel, C.,  
20 Boubrahmi, N. F., Font, J., Grubišić, V., Gualdi, S., Homar, V., Ivančan-Picek, B., Kottmeier, C., Kotroni, V., Lagouvardos, K., Lionello, P., Llasat, M. C., Ludwig, W., Lutoff, C., Mariotti, A., Richard, E., Romero, R., Rotunno, R., Roussot, O., Ruin, I., Somot, S., Taupier-Letage, I., Tintore, J., Uijlenhoet, R., and Wernli, H.: HyMeX: A 10-Year Multidisciplinary Program on the Mediterranean Water Cycle, *Bulletin of the American Meteorological Society*, 95, 1063–1082, <https://doi.org/10.1175/BAMS-D-12-00242.1>, 2014.
- Drobinski, P., Alonzo, B., Bastin, S., Da Silva, N., and Muller, C.: Scaling of precipitation extremes with temperature in the  
25 French Mediterranean region: What explains the hook shape?, *Journal of Geophysical Research: Atmospheres*, 121, 3100–3119, <https://doi.org/10.1002/2015JD023497>, 2016.
- Drobinski, P., Da Silva, N., Panthou, G., Bastin, S., Muller, C., Ahrens, B., Borga, M., Conte, D., Fossier, G., Giorgi, F., Güttler, I., Kotroni, V., Li, L., Morin, E., Öno, B., Quintana-Segui, P., Romera, R., and Torma, C. Z.: Scaling precipitation extremes with temperature in the Mediterranean: past climate assessment and projection in anthropogenic scenarios, *Climate Dynamics*, 51, 1237–1257, <https://doi.org/10.1007/s00382-016-3083-x>, 2018.
- 30 Fan, J., Leung, L. R., Rosenfeld, D., Chen, Q., Li, Z., Zhang, J., and Yan, H.: Microphysical effects determine macrophysical response for aerosol impacts on deep convective clouds, *Proceedings of the National Academy of Sciences*, 110, E4581–E4590, <https://doi.org/10.1073/pnas.1316830110>, <http://www.pnas.org/content/110/48/E4581.abstract>, 2013.
- Ginoux, P., Chin, M., Tegen, I., Prospero, J. M., Holben, B., Dubovik, O., and Lin, S.-J.: Sources and distributions of dust aerosols simulated  
35 with the GOCART model, *Journal of Geophysical Research: Atmospheres*, 106, 20 255–20 273, <https://doi.org/10.1029/2000JD000053>, 2001.



- Haerter, J. O. and Berg, P.: Unexpected rise in extreme precipitation caused by a shift in rain type?, *Nature Geoscience*, 2, 372, <https://doi.org/10.1038/ngeo523>, correspondence, 2009.
- Hardwick, J. R., Westra, S., and Sharma, A.: Observed relationships between extreme sub-daily precipitation, surface temperature, and relative humidity, *Geophysical Research Letters*, 37, <https://doi.org/10.1029/2010GL045081>, 2010.
- 5 Held, I. M. and Soden, B. J.: Robust Responses of the Hydrological Cycle to Global Warming, *Journal of Climate*, 19, 5686–5699, <https://doi.org/10.1175/JCLI3990.1>, 2006.
- Iacono, M. J., Delamere, J. S., Mlawer, E. J., Shephard, M. W., Clough, S. A., and Collins, W. D.: Radiative forcing by long-lived greenhouse gases: Calculations with the AER radiative transfer models, *Journal of Geophysical Research: Atmospheres*, 113, n/a–n/a, <https://doi.org/10.1029/2008JD009944>, d13103, 2008.
- 10 Kain, J. S.: The Kain–Fritsch Convective Parameterization: An Update, *Journal of Applied Meteorology*, 43, 170–181, [https://doi.org/10.1175/1520-0450\(2004\)043<0170:TKCPAU>2.0.CO;2](https://doi.org/10.1175/1520-0450(2004)043<0170:TKCPAU>2.0.CO;2), 2004.
- Lelieveld, J., Berresheim, H., and Borrmann, S.: Global air pollution crossroads over the Mediterranean., *Science*, 298, 794–799, <https://doi.org/10.1126/science.1075457>, 2002.
- Lenderink, G. and van Meijgaard, E.: Increase in hourly precipitation extremes beyond expectations from temperature changes, *Nature*
- 15 *Geoscience*, 1, 511, 2008.
- Lenderink, G., Barbero, R., Loriaux, J. M., and Fowler, H. J.: Super-Clausius–Clapeyron Scaling of Extreme Hourly Convective Precipitation and Its Relation to Large-Scale Atmospheric Conditions, *Journal of Climate*, 30, 6037–6052, <https://doi.org/10.1175/JCLI-D-16-0808.1>, <https://doi.org/10.1175/JCLI-D-16-0808.1>, 2017.
- Lenka, C. and Eva, H.: Simulated relationship between air temperature and precipitation over Europe: sensitivity to the choice of RCM and
- 20 GCM, *International Journal of Climatology*, 38, 1595–1604, <https://doi.org/10.1002/joc.5256>, 2017.
- Li, F., Collins, W. D., Wehner, M. F., Williamson, D. L., Olson, J. G., and Algieri, C.: Impact of horizontal resolution on simulation of precipitation extremes in an aqua-planet version of Community Atmospheric Model (CAM3), *Tellus A: Dynamic Meteorology and Oceanography*, 63, 884–892, 2011.
- Loriaux, J. M., Lenderink, G., De Roode, S. R., and Siebesma, A. P.: Understanding Convective Extreme Precipitation Scaling Using Observations and an Entraining Plume Model, *Journal of the Atmospheric Sciences*, 70, 3641–3655, <https://doi.org/10.1175/JAS-D-12-0317.1>, 2013.
- Madden, R. A. and Williams, J.: The correlation between temperature and precipitation in the United States and Europe, *Monthly Weather Review*, 106, 142–147, [https://doi.org/10.1175/1520-0493\(1978\)106<0142:TCBTAP>2.0.CO;2](https://doi.org/10.1175/1520-0493(1978)106<0142:TCBTAP>2.0.CO;2), 1978.
- Molnar, P., Fatichi, S., Gaál, L., Szolgay, J., and Burlando, P.: Storm type effects on super Clausius–Clapeyron scaling of intense rainstorm
- 30 properties with air temperature, *Hydrology and Earth System Sciences*, 19, 1753–1766, <https://doi.org/10.5194/hess-19-1753-2015>, 2015.
- Morrison, H. and Grabowski, W. W.: Cloud-system resolving model simulations of aerosol indirect effects on tropical deep convection and its thermodynamic environment, *Atmospheric Chemistry and Physics*, 11, 10 503–10 523, <https://doi.org/10.5194/acp-11-10503-2011>, 2011.
- National Centers for Environmental Prediction National Weather Service, NOAA, U. D. o. C.: NCEP FNL Operational Model Global Tropospheric Analyses, continuing from July 1999, <https://doi.org/10.5065/D6M043C6>, 2000.
- 35 Omrani, H., Drobinski, P., and Dubos, T.: Optimal nudging strategies in regional climate modelling: investigation in a Big–Brother experiment over the European and Mediterranean regions, *Climate Dynamics*, 41, 2451–2470, <https://doi.org/10.1007/s00382-012-1615-6>, 2013.
- Omrani, H., Drobinski, P., and Dubos, T.: Using nudging to improve global-regional dynamic consistency in limited-area climate modeling: What should we nudge?, *Climate Dynamics*, 44, 1627–1644, <https://doi.org/10.1007/s00382-014-2453-5>, 2015.



- Panthou, G., Mailhot, A., Laurence, E., and Talbot, G.: Relationship between Surface Temperature and Extreme Rainfalls: A Multi-Time-Scale and Event-Based Analysis, *Journal of Hydrometeorology*, 15, 1999–2011, <https://doi.org/10.1175/JHM-D-14-0020.1>, 2014.
- Ramanathan, V., Crutzen, P. J., Kiehl, J. T., and Rosenfeld, D.: Aerosols, Climate, and the Hydrological Cycle, *Science*, 294, 2119–2124, <https://doi.org/10.1126/science.1064034>, 2001.
- 5 Rodrigo, F. S.: Coherent variability between seasonal temperatures and rainfalls in the Iberian Peninsula, 1951–2016, *Theoretical and Applied Climatology*, <https://doi.org/10.1007/s00704-018-2400-1>, 2018.
- Salameh, T., Drobinski, P., and Dubos, T.: The effect of indiscriminate nudging time on large and small scales in regional climate modelling: Application to the Mediterranean basin, *Quarterly Journal of the Royal Meteorological Society*, 136, 170–182, <https://doi.org/10.1002/qj.518>, 2010.
- 10 Salzmann, M., Weser, H., and Cherian, R.: Robust response of Asian summer monsoon to anthropogenic aerosols in CMIP5 models, *Journal of Geophysical Research: Atmospheres*, 119, 11,321–11,337, <https://doi.org/10.1002/2014JD021783>, 2014.
- Seifert, A., Heus, T., Pincus, R., and Stevens, B.: Large-eddy simulation of the transient and near-equilibrium behavior of precipitating shallow convection, *Journal of Advances in Modeling Earth Systems*, 7, 1918–1937, <https://doi.org/10.1002/2015MS000489>, 2015.
- Singh, M. S. and O’Gorman, P. A.: Influence of microphysics on the scaling of precipitation extremes with temperature, *Geophysical Research Letters*, 41, 6037–6044, <https://doi.org/10.1002/2014GL061222>, 2014.
- 15 Singleton, A. and Toumi, R.: Super-Clausius–Clapeyron scaling of rainfall in a model squall line, *Quarterly Journal of the Royal Meteorological Society*, 139, 334–339, <https://doi.org/10.1002/qj.1919>, 2013.
- Skamarock, W., Klemp, J., Dudhia, J., Gill, D., Barker, D., Wang, W., Huang, X.-y., Duda, M., and Powers, J.: A Description of the Advanced Research WRF Version 3, NCAR Tech. Note NCAR/TN-475+STR, <https://doi.org/10.5065/D68S4MVH>, 113 pp., 2008.
- 20 Small, J. D., Chuang, P. Y., Feingold, G., and Jiang, H.: Can aerosol decrease cloud lifetime?, *Geophysical Research Letters*, 36, n/a–n/a, <https://doi.org/10.1029/2009GL038888>, 116806, 2009.
- Stevens, B. and Feingold, G.: Untangling aerosol effects on clouds and precipitation in a buffered system, *Nature*, 461, 607–613, <https://doi.org/10.1038/nature08281>, 2009.
- Tegen, I., Hollrig, P., Chin, M., Fung, I., Jacob, D., and Penner, J.: Contribution of different aerosol species to the global aerosol extinction optical thickness: Estimates from model results, *Journal of Geophysical Research: Atmospheres*, 102, 23 895–23 915, <https://doi.org/10.1029/97JD01864>, 1997.
- 25 Thompson, G. and Eidhammer, T.: A Study of Aerosol Impacts on Clouds and Precipitation Development in a Large Winter Cyclone, *Journal of the Atmospheric Sciences*, 71, 3636–3658, <https://doi.org/10.1175/JAS-D-13-0305.1>, 2014.
- Trenberth, K. E.: Atmospheric Moisture Residence Times and Cycling: Implications for Rainfall Rates and Climate Change, *Climatic Change*, 39, 667–694, <https://doi.org/10.1023/A:1005319109110>, 1998.
- 30 Trenberth, K. E. and Shea, D. J.: Relationships between precipitation and surface temperature, *Geophysical Research Letters*, 32, <https://doi.org/10.1029/2005GL022760>, 2005.
- Twomey, S.: The Influence of Pollution on the Shortwave Albedo of Clouds, *Journal of the Atmospheric Sciences*, 34, 1149–1152, [https://doi.org/10.1175/1520-0469\(1977\)034<1149:TIOPO>2.0.CO;2](https://doi.org/10.1175/1520-0469(1977)034<1149:TIOPO>2.0.CO;2), 1977.
- 35 Utsumi, N., Seto, S., Kanae, S., Maeda, E. E., and Oki, T.: Does higher surface temperature intensify extreme precipitation?, *Geophysical Research Letters*, 38, <https://doi.org/10.1029/2011GL048426>, 2011.
- Zhao, W. and Khalil, M. A. K.: The Relationship between Precipitation and Temperature over the Contiguous United States, *Journal of Climate*, 6, 1232–1236, [https://doi.org/10.1175/1520-0442\(1993\)006<1232:TRBPAT>2.0.CO;2](https://doi.org/10.1175/1520-0442(1993)006<1232:TRBPAT>2.0.CO;2), 1993.



Zhou, C. and Penner, J. E.: Why do general circulation models overestimate the aerosol cloud lifetime effect? A case study comparing CAM5 and a CRM, *Atmospheric Chemistry and Physics*, 17, 21–29, <https://doi.org/10.5194/acp-17-21-2017>, 2017.